Journal of
Marine Science
and Engineering

Article

One-Dimensional Solar Energy Thermal Consolidation Model Testing and Analytical Calculation for Marine Soft Clays

Changqing Xia [1], Yuebao Deng [2], Min Zhu [1,*], Jiajun Niu [3], Liangke Zheng [2] and Xiangsheng Chen [1]

[1] College of Civil and Transportation Engineering, Shenzhen University, Shenzhen 518061, China
[2] Institute of Geotechnical Engineering, Ningbo University, Ningbo 315211, China
[3] China Construction Infrastructure Co., Ltd., Beijing 100022, China
* Correspondence: zhuminfnf@szu.edu.cn

Abstract: There are significant energy and financial expenditures associated with the current thermal drainage consolidation approach used to treat the marine soft clay foundation. Especially for some reclaimed lands in remote areas where a large amount of stable electricity is not readily available. In view of the problem, this paper aims to investigate a novel treatment method by using solar energy thermal consolidation. The model testing was conducted to assess the treatment effect of the foundation. Results from two groups of one-dimensional surcharge preloading consolidation model experiments, conducted under conditions of both solar heating and ambient temperature, were presented. The advantage of the solar heating approach was demonstrated by a comparison of the two tests. An analytical calculation method was proposed for predicting the consolidation behavior on the basis of the temperature variation caused by solar energy in the marine soft clays, and good agreement was observed. The outcomes reveal that solar heating can improve the consolidation effect of soil deep in the foundation. The foundation temperature can be raised by 15 °C in winter, and the variation range can exceed 10 °C. The settlement increases by 16% compared with the ambient temperature group.

Keywords: solar energy; thermal consolidation; marine soft clays; model testing; analytical calculation

Citation: Xia, C.; Deng, Y.; Zhu, M.; Niu, J.; Zheng, L.; Chen, X. One-Dimensional Solar Energy Thermal Consolidation Model Testing and Analytical Calculation for Marine Soft Clays. *J. Mar. Sci. Eng.* **2022**, *10*, 1634. https://doi.org/10.3390/jmse10111634

Academic Editor: George Kontakiotis

Received: 16 September 2022
Accepted: 29 October 2022
Published: 2 November 2022

1. Introduction

Due to a lack of available land, many coastal cities must perform land reclamation from tidal flats or by hydraulic fills. These lands will present significant post-construction settlement issues for projects such as buildings, airports, ports, and other structures. Construction periods frequently take up 30% to 40% of the overall construction period when treating soft soil foundations. It has been a hot topic among academics all over the world to address marine soft soil foundation in a more efficient and inexpensive manner to hasten its consolidation [1–3]. The coefficient of consolidation is correlated with temperature, according to research from the 1950s. The value of the coefficient of consolidation increases by roughly twofold as the temperature increases by 4.4 °C to 21.1 °C [4]. This is explained by the fact that as the temperature rises, the viscosity coefficient of pore fluid drops [5], leading to an increased permeability coefficient [6–8]. On the other hand, as the temperature rises, the soil skeleton around the area constrains the pore fluid's thermal expansion, which leads to an increase in pore water pressure [9–11]. Greater permeability will result from higher temperatures, and the excess pore water pressure they cause will dissipate more quickly as a result [8]. Theoretical and experimental research on the thermal consolidation of soft soil has been conducted based on the thermodynamic properties of soft soil [12–19].

The first embankment field tests on the thermal consolidation treatment of Bangkok soft soil by employing the drainage plate with heating devices were conducted by Pothiraksanon et al. [20], and they showed that this method yields more settlement and a higher rate of consolidation. Bai et al. [21] conducted a temperature-controlled triaxial test to examine the differences in pore water pressure and consolidation volume strain brought on by varying temperature amplitudes and confining pressures. They discovered that the maximum pore water pressure and consolidation volume strain increased with the rise in temperature amplitude. In the theoretical research of thermal consolidation, Bai et al. [22] provided the solution of one-dimensional thermal consolidation where one side of saturated single-layer soil is permeable and can conduct heat exchange by the Fourier transform. Liu et al. [23] established a one-dimensional nonlinear consolidation theory, taking into account secondary consolidation and the thermal effect, and simplified the temperature effect as the translation of the e-log p curve. The precise solutions for one-dimensional thermal consolidation were presented by Niu et al. [24], who also considered thermo-osmosis and thermo-filtration. Tao et al. [25] presented both the differential form and weak form of control equations, and established a finite element model in COMSOL to investigate the thermos-hydro-mechanical effect of consolidation.

Scholars have expended considerable effort in researching the mechanical mechanism of thermal consolidation by means of experimentation and theoretical investigation [26–34]. To expand this foundation treatment technology, the relevant heating devices have been invented, improved, and applied in actual engineering. However, it is only used in some urgent projects because traditional high-temperature electric heating technology comes with high energy consumption and costs, as well as potential safety issues. Furthermore, the reclaimed lands are usually located in remote areas with limited access to dependable electricity. These factors have hampered the spread of technology. In view of this, a novel foundation treatment method based on solar energy thermal consolidation will be investigated in this paper. The temperature fluctuations in soil, the generation and dissipation of thermal excess pore water pressure, and settlement will be presented and analyzed using the one-dimensional consolidation model testing by solar heating in combination with surcharge loading. Finally, analytical solutions will be developed and compared to the testing results.

2. Description of Model Testing

2.1. Soil and Test Sites Climatic Conditions

The clays employed in this study were obtained from Ningbo, a city in China's Zhejiang province, as shown in Figure 1. The sample is a typical marine clay deposit made up of muck and silt from the East China Sea. In order to make the soil sample homogenous and to prepare it for a normal consolidation state, the clays were stirred, and the impurities, such as gravel blocks, were removed before the test. Table 1 displays some of the soil's basic physical properties. The test sites' annual average temperature when conducting tests is 18.5 °C, 1.5 °C above the perennial average temperature in Ningbo. There are 1515.4 h of sunshine throughout the year, 14% less than the perennial average sunshine duration. Additionally, there are more sunshine hours in January, September, and December.

2.2. Experimental Devices

The test equipment, as depicted in Figure 2, consisted of a model tank, a solar hot water circulation system, a drainage and water charging system, and a loading system. The stainless steel model tank had dimensions of 100 cm by 50 cm by 120 cm (length, width, and height), and a layer of thermal insulation material was applied to its exterior surface. The components of the solar hot water circulation system were a solar water heater, a water tank, a water pump, and metal bellows for heat transfer. For circulation, tubes were used to connect these devices. A sand cushion that was placed on the ground serves as the drainage boundary. The pore water penetrates the sand cushion under the pore pressure gradient when loading was applied. The basic function of the water charging system was to imitate groundwater recharging for a constant groundwater level.

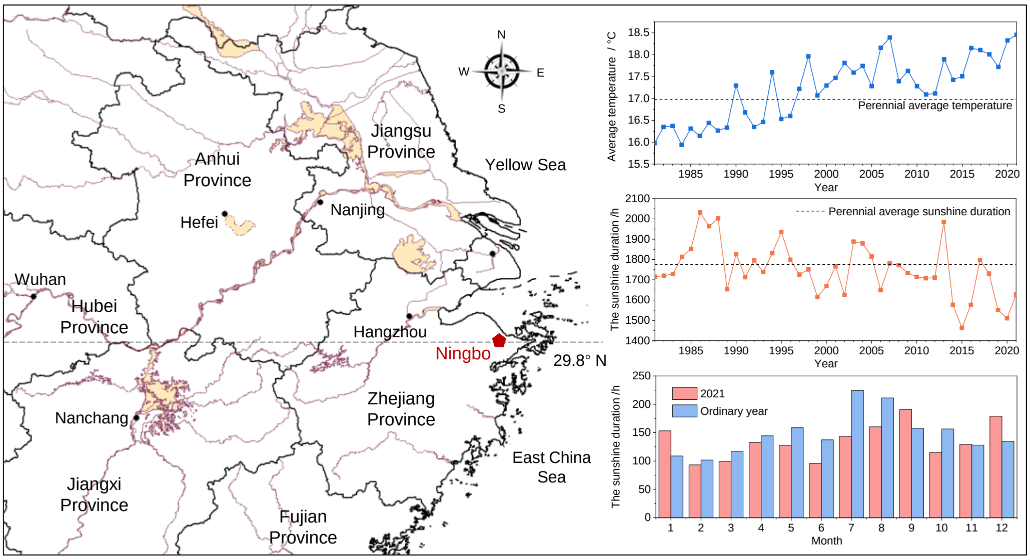

Figure 1. Sampling and test sites climatic conditions.

Table 1. Soil parameters in laboratory tests.

d_s	w/%	ρ/g/cm^3	e	E_s
2.72	40.87	1.73	1.22	0.9

Note: d_s = specific gravity; w = water content; ρ = natural density; e = void ratio; E_s = modulus of compressibility.

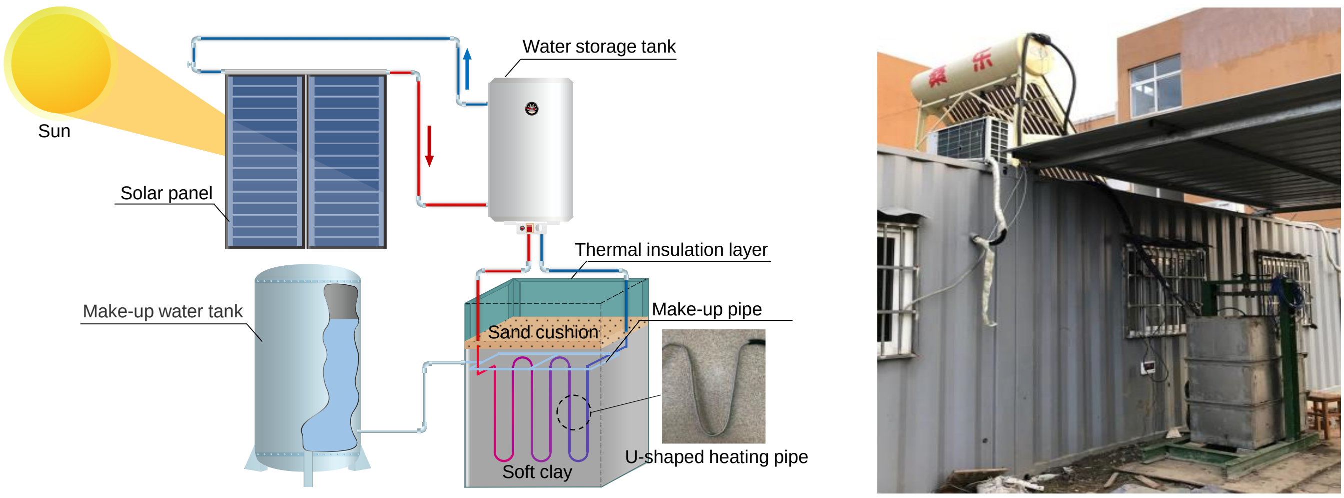

(**a**) (**b**)

Figure 2. Schematic diagram of test model device. (**a**) Schematic diagram of test model device; (**b**) physical diagram of the test model device.

A perforated cover plate, jack, reaction frame, and lever complete the loading system. The cover plate, as shown in Figure 3, was 95 cm × 45 cm × 1 cm (length × wide × thick). It had 8 small holes, each with a diameter of 2 cm, to prevent interfering with the sand cushion's drainage ability. The cover plate was rigid enough, which allowed the force in the soil to be distributed more evenly. As seen in Figure 4, the jack serves as the lever's fulcrum, whose position was the middle of the cover plate. The lever's 10:1 length-to-arm ratio allows for continuous loading while also reducing the number of weights required.

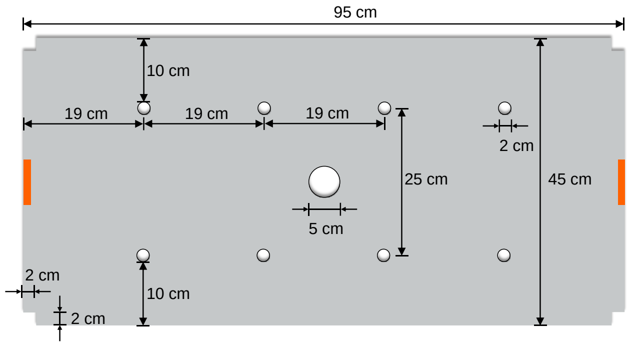

Figure 3. Hole cover plate.

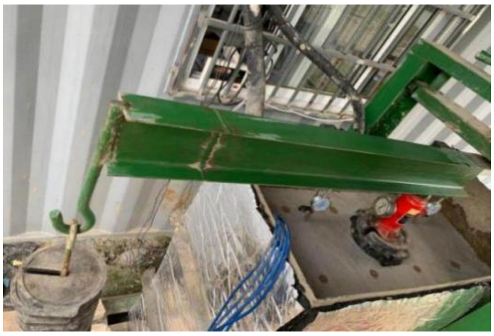

Figure 4. Loading system.

2.3. Measuring Equipment

Figure 5 depicts the measuring equipment, which includes pore water pressure gauges, dial gauges, and thermometers. On either side of the model foundation, two dial gauges were symmetrically positioned to measure the settlement. The employment of a long metal rod with a chassis helped to prevent the error brought on by the settlement of the sand cushion. The lower end of the rod met the top of the soil layer, while the upper end served as the dial indicator's measuring point. The mean value of the measured settlement data was taken as the surface settlement. During the testing, a YH04–A06 vibrating wire temperature integrated pore water pressure gauge with water pressure sensitive integrated components was used. The sensor was 26 mm $\times$ 200 mm in size, had a pore water pressure range of 0–0.1 MPa, and the error was 0.1 kPa. The temperature range was -20 to 80 °C, with a total error of less than 0.2% FS. Simultaneously, a data display instrument customized for vibrating wire sensors was configured.

2.4. Tests Procedure

Two groups of model testing were planned to examine the effect of solar energy combined with the surcharge preloading method: the one-dimensional drainage consolidation model test at ambient temperature and under solar heating circumstances. The former involved laying a sand cushion on the surface to create one-dimensional drainage conditions, while the latter employed solar energy to heat the water that forms circulation to heat the soil. The heat distribution and development change generated by solar energy in the foundation were tested during the test, and the pore water pressure and settlement development process were monitored to determine the effect of solar heating on the consolidation behavior.

The U-shaped heat transfer metal bellows were embedded in the model tank, and Figure 6 illustrates where the heat transfer pipe was located. Clays were then filled to the model tank using the layered compaction technique. The clays were filled with four layers, and the virtual height of each layer was 30 cm. The cover plate was positioned on the surface of each filled layer with weight and preloaded with 1 kPa until the settlement of the filled layer was steady. After that, the following layer was filled. When the last layer of clay was filled, the preloading with 1 kPa was applied for seven days after the layer had reached a filling height of 100 cm. The sensor was buried into the target position of the clay after the process of filling the clay was finished in order to prevent the position change of the pore water pressure gauge caused by the soil squeezing action during preloading. A thin-walled steel tube coated with Vaseline was slowly inserted into the clay to the design depth of the sensor buried, and then the sensor was buried after being excavated. Following that, the clay was mashed into small pieces and filled into the borehole before being tamped with wooden sticks in layers. Figure 6a,b depict the placement of the pore water pressure gauge in the ambient temperature group and solar heating group, respectively. The pore water pressure and temperature distribution laws of various drainage distances and various heat source distances can be measured by implementing the aforementioned embedding approach.

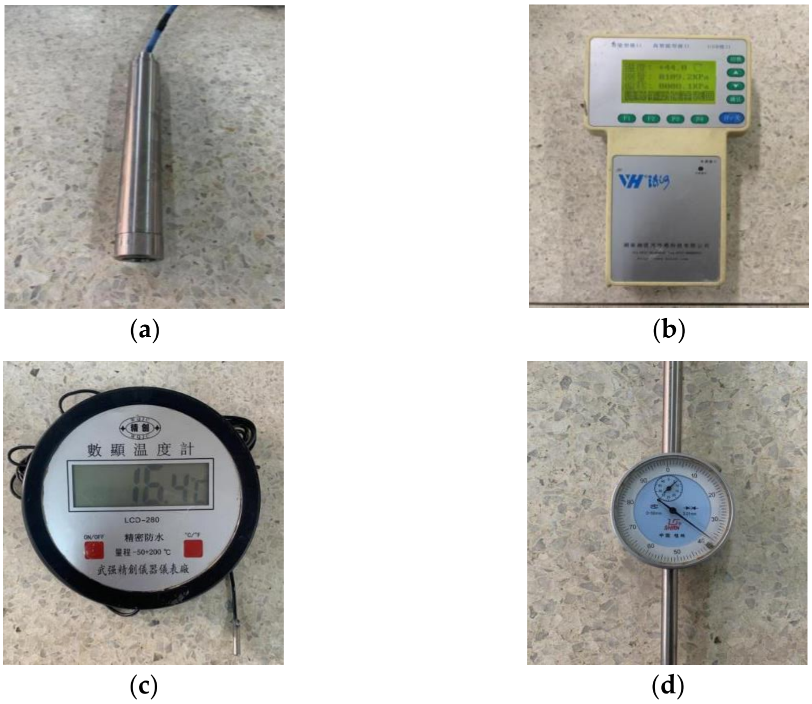

Figure 5. Measuring equipment. (**a**) Pore water pressure gauge; (**b**) digital display instrument; (**c**) thermometer; (**d**) dial gage.

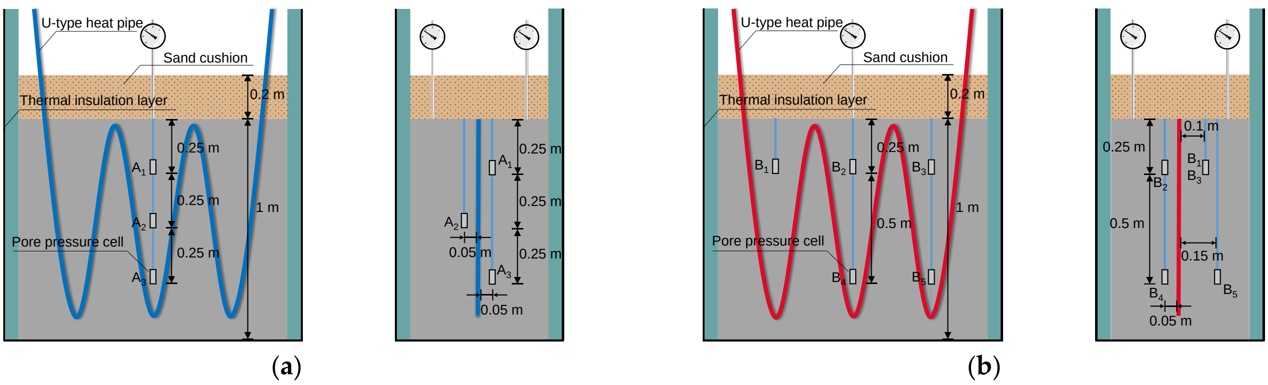

Figure 6. Location of pore water pressure gauge. (**a**) Ambient temperature group; (**b**) solar heating group.

The sand cushion, whose design thickness was 20 cm, was placed atop the soft clays after the pore water pressure gauge had been embedded. To prevent uneven loading and differential settlement, a leveling tool was employed. The multistage loading levels, which are applied by weight and leverage, were 2.5 kPa, 12.5 kPa, and 25 kPa, respectively.

The settlement was measured and read at intervals of 10 min, 10 min, 10 min, 15 min, and 15 min, after that, measurements were taken at 30 min intervals. When the hourly settlement dropped to less than 0.1 mm over the course of two hours, it was regarded to have stabilized and progressed to the next level of load. Water circulation was opened concurrently with loading during the solar heating group's test, and variations in soil temperature and pore water pressure were continuously tracked.

3. Testing Result and Discussion

3.1. Temperature

Figure 7 shows the soil temperature change with time for both the ambient temperature and the solar heating groups. According to Figure 7a, the soil temperature was comparatively steady without heating, with an average daily temperature variation of about 2 °C. The foundation soil's starting temperature was low since the heating group test was conducted in the winter. Due to weather differences, the test did not take place in perfect sunshine every day, which caused the temperature in the soil to vary without considerable regularity in Figure 7b. It can be noted that the daily average temperature throughout the solar heating process is 5 °C, whereas the average temperature of clays was 20 °C, with an overall increase of roughly 15 °C. Even though it dropped over the night, the soil temperature never returned to its starting point. The primary causes were the high specific heat of water, delayed temperature decline, and retarded heat dissipation of soil under the impact of the thermal insulating layer. The absence of a heat source in the ambient temperature group accounted for the soil's generally average temperature distribution. In the solar heating group, the soil temperature and distance from the heat source were inversely correlated, and as the distance from the heat source increases, so does the heat transmission. In the solar heating group, the daily temperature difference at some locations in the soil could even reach 10.6 °C, which was much higher than in the ambient temperature group. It was clear that solar heating could enhance the range of temperature fluctuation during cyclic temperature change in addition to improving the soil's average temperature.

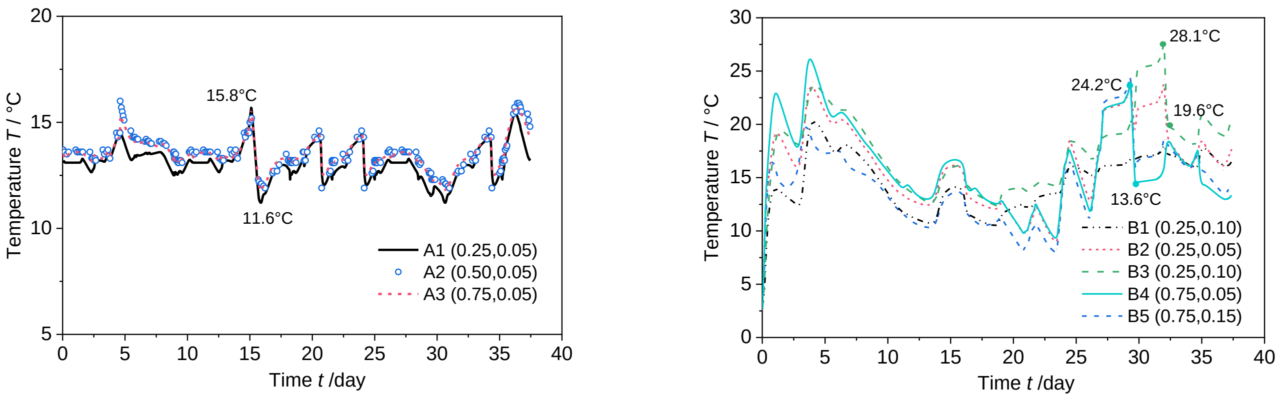

Figure 7. Temperature curves with time. (**a**) Ambient temperature group; (**b**) solar heating group.

3.2. Pore Water Pressure

Figure 8 shows the time-dependent change curves for the excess pore water pressure in the ambient temperature and solar heating groups. As illustrated in Figure 8a, in the absence of a heat source, pore water pressure tended to progressively diminish. In contrast, the heating group had a significant difference in the variation trend of pore water pressure, as shown in Figure 8b. The primary cause of the discrepancy was the influence of heating, which can raise soil pore water pressure. The temperature was the only factor that contributed to the rise in pore water pressure in the later stage of loading. The average pore water pressure increased by 2.5 kPa in a single day, and the maximum pore water pressure rise caused by heating was 6.8 kPa. On a sunny day, the excess pore water pressure began to increase at about 7:00 as the sun rose and reached its peak at 15:20 as the sun was ready to set and the temperature began to decrease. Surely, the increased pore water pressure was mainly caused by the thermal expansion of the pore water. When the temperature raised, the pore water expanded as did the clay skeleton. Both resulted in an increase in total stress as a result of the lateral displacement constraint imposed by the tank's wall, so as to cause clay consolidation.

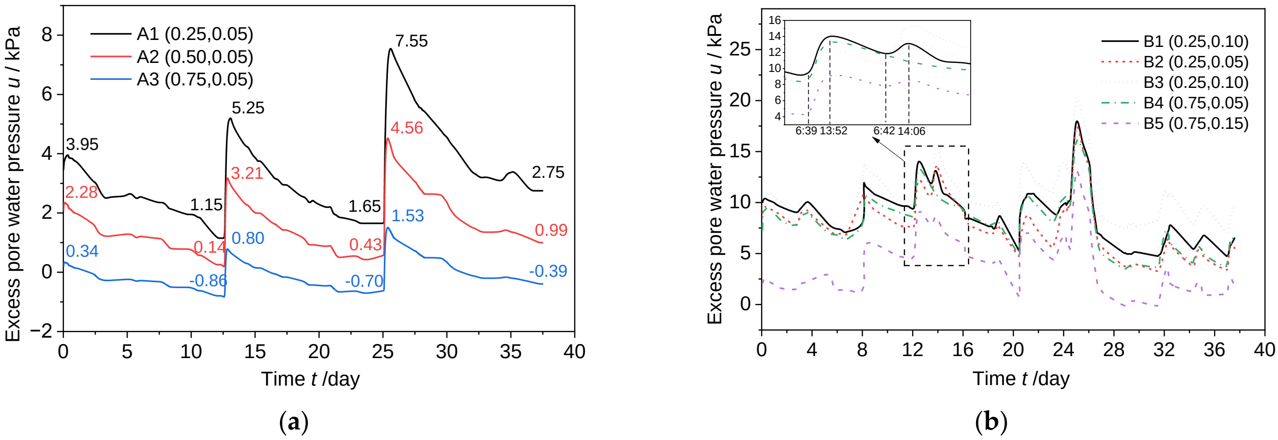

Figure 8. Excess pore water pressure curves with time. (**a**) Ambient temperature group; (**b**) solar heating group.

A1 in the ambient temperature group was the shallowest, and the pore water pressure variation range was the most pronounced. The range of pore water pressure variation gradually decreased as depth increased. The effectiveness of load downward transfer was weakened by the effect of model tank wall friction, which was the main cause. This phenomenon may be seen in engineering as well, and it highlighted the drawback that preloading methods had in that their reinforcement impact decreases with depth. While the single-day excess pore water pressure gradient remained considerable in the solar heating group to a depth of 75 cm, which suggested that solar heating can enhance the drainage efficiency of deep areas in the soil. It was clear that the drainage distance affects how quickly excess pore water pressure dissipated. The shorter the drainage distance, the faster the excess pore water pressure dissipated.

3.3. Settlement

The development of the foundation settlement with time in the two groups of model testing is depicted in Figure 9. The settlement change pattern in the ambient temperature group was identical to that of the solar heating group. The settlement rate exhibits a progressive slowing tendency prior to the application of the following stage loading. After 36 days of loading, the overall settlement for the ambient temperature group was 25.0 mm and 29.1 mm for the solar heating group. The solar heating group's settlement was 16% higher than the ambient group's. The two groups' settlements varied by 1.2 mm under a first-stage loading of 2.5 kPa. The difference between the two groups was 3.1 mm under the second-stage loading of 12.5 kPa. The two groups' settlements differ by 4.1 mm under a third-stage loading of 25 kPa. It was clear that as drainage consolidation advanced, the impact of solar heating on accelerating foundation settlement steadily increased. Figure 10 shows the settlement rate with time. The settlement rate increased immediately after reloading before beginning to decrease. The rate increased all night, but dropped during the day. This phenomenon could be attributed to the consolidation during the night, partly to the thermal contraction of the clay.

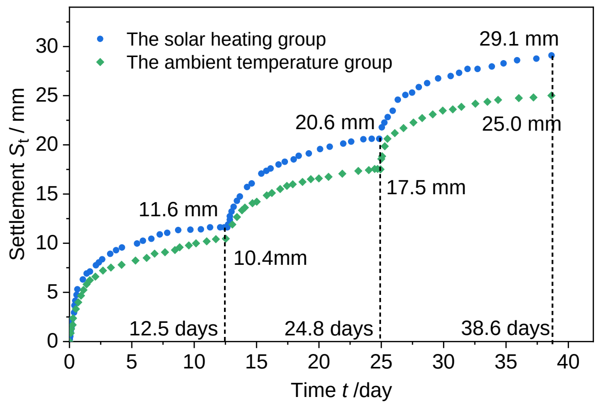

Figure 9. Settlement with time.

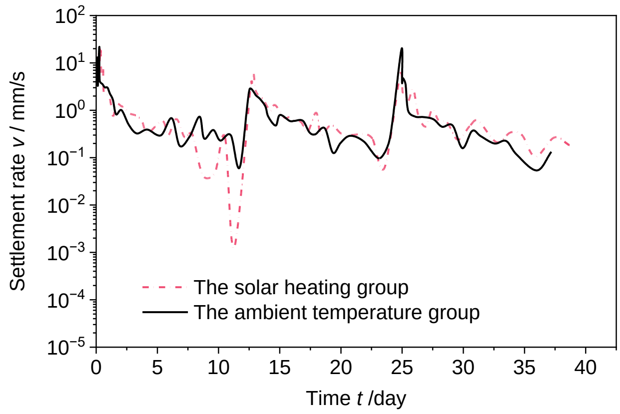

Figure 10. Settlement rate with time.

4. Analytical Calculation

In this section, based on the aforementioned testing results, an analytical calculation method was rendered for predicting the behavior of solar energy thermal consolidation. By comparing with testing results, the analytical calculating results can be verified.

4.1. Computational Model

The strata model for one-dimensional thermal consolidation of saturated soft clay is shown in Figure 11. The total thickness of the soil strata is H. Idealized single-drainage situations equate to the top surface being fully pervious and the bottom surface being fully impervious. On the top surface, a time-dependent load, $q(t)$, is applied. Seepage complies with Darcy's law, and temperature conduction follows Fourier's law. The physical parameters of soil are taken to be constant during the thermal consolidation process.

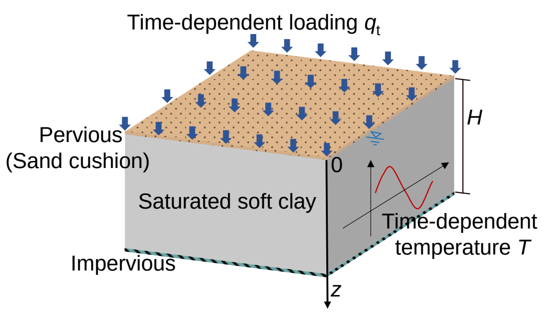

Figure 11. The strata model of saturated soft clay.

4.2. Governing Equations

Based on the theory for thermal consolidation of soil [35], the governing equations for one-dimensional thermal consolidation of saturated soft clay under time-dependent load can be given as

$$\begin{cases} \frac{\partial^2 u(z,t)}{\partial z^2} = A_1 \frac{\partial u(z,t)}{\partial t} + A_2 \frac{\partial T(z,t)}{\partial t} + A_3 \frac{\partial q(t)}{\partial t} \\ \frac{\partial^2 T(z,t)}{\partial z^2} = A_4 \frac{\partial T(z,t)}{\partial t} \end{cases} \tag{1}$$

where $A_1 = \frac{1/E_s + n/K_w + (1-n)/K_s}{k_w/\gamma_w}$, $A_2 = \frac{3K_0\alpha_s/E_s - 3[(1-n)\alpha_s + n\alpha_w]}{k_w/\gamma_w}$, $A_3 = \frac{\gamma_w}{k_w E_s}$, $A_4 = \frac{K_T}{c}$, where k_w is the coefficient of permeability; E_s is compression modulus; γ_w is the unit weight of water; n is void ratio; α_s and α_w represent the coefficient of thermal expansion of soil particles and pore water, respectively; K_0 is the bulk modulus of soil skeleton; K_s is the bulk modulus of soil particles; K_w is the bulk modulus of pore water; K_T is the coefficient of thermal conduction; c is the specific heat capacity of unit volume.

If the temperature change is known, the governing equations in terms of excess pore pressure can be simplified as

$$\frac{\partial^2 u(x,t)}{\partial x^2} = A_1 \frac{\partial u(x,t)}{\partial t} + f(t) \tag{2}$$

where $f(t)$ is the external cause of excess pore pressure change, including loading and heat transmission.

The boundary conditions corresponding to the governing equations can be expressed by the following equations:

$$z = 0 \quad u = 0 \quad \text{(pervious top boundary)} \tag{3}$$

$$z = H \quad \frac{\partial u}{\partial z} = 0 \quad \text{(impervious bottom boundary)} \tag{4}$$

The initial condition for excess pore water pressure is expressed as follows:

$$t = 0 \quad u = u_0 \tag{5}$$

where u_0 is the initial excess pore water pressure caused by heating up.

4.3. Solutions

The method of separating variables is used to get the characteristic function of the differential Equation (2). The homogeneous form of the governing Equation (2) is

$$\frac{\partial^2 u(z,t)}{\partial z^2} = A_1 \frac{\partial u(z,t)}{\partial t} \tag{6}$$

Assuming that the solution of the pore water pressure is

$$u(z,t) = Y(t) \cdot X(z) \tag{7}$$

$$\frac{X_{,zz}(z)}{X(z)} = A_1 \frac{Y_{,t}(t)}{Y(t)} = -\omega^2 \tag{8}$$

where ω is a non-negative real number.

According to Equation (8),

$$X(z) = c_1 \sin(\omega \cdot z) + c_2 \cos(\omega \cdot z) \tag{9}$$

where c_1 and c_2 are undetermined constants.

After substituting Equation (9) into the boundary conditions (3) and (4), it can be obtained that

$$c_1 \cdot \cos(\omega \cdot H) = 0 \tag{10}$$

$$c_2 = 0 \tag{11}$$

The kth solution of ω in Equation (10) can be expressed as follows:

$$\omega_k = \frac{(2k-1)\pi}{2H} \tag{12}$$

As a result, the characteristic function can be obtained as

$$X_k(z) = \sin\left(\frac{2k-1}{2H}\pi z\right) \tag{13}$$

According to the characteristic function expansion method, it is assumed that the solution of the differential Equation (2) is

$$u(x,t) = \sum_{k=1}^{\infty} Y_k(t)\sin\left(\frac{2k-1}{2H}\pi z\right) = \sum_{k=1}^{\infty} Y_k(t)\sin(\omega_k z) \tag{14}$$

Substitution of Equation (14) into Equation (2) gives

$$-\sum_{k=1}^{\infty} \omega_k^2 Y_k(t)\sin(\omega_k x) = A_1\sum_{k=1}^{\infty} Y_{k,t}(t)\sin(\omega_k x) + f(t) \tag{15}$$

According to the orthogonality of trigonometric function, it can be obtained as

$$-\int_0^H \sum_{k=1}^{\infty} \omega_k^2 Y_k(t)\sin(\omega_k z)\sin(\omega_i z)\mathrm{d}z = A_1\int_0^H \sum_{k=1}^{\infty} Y_{k,t}(t)\sin(\omega_k z)\sin(\omega_i z)\mathrm{d}z + \int_0^H f(t)\sin(\omega_i z)\mathrm{d}z \tag{16}$$

Then

$$Y_{k,t}(t) = -\frac{\omega_k^2}{A_1}\cdot Y_k(t) - \frac{2}{H\cdot A_1\cdot\omega_k}\cdot f(t) \tag{17}$$

The solution of Equation (17) can be expressed as:

$$Y_k(t) = e^{-\frac{\omega_k^2}{A_1}t}Y_k(0) + e^{-\frac{\omega_k^2}{A_1}t}\int_0^t e^{\frac{\omega_k^2}{A_1}\xi}\cdot\left(-\frac{2}{H\cdot A_1\cdot\omega_k}\cdot f(\xi)\right)\mathrm{d}\xi \tag{18}$$

According to the initial condition, it can be obtained that

$$u(z,0) = \sum_{k=1}^{\infty} Y_k(0)\sin(\omega_k z) = u_0 \tag{19}$$

By multiplying $\sin(\omega_i z)$ on both sides of Equation (19) and integrating z form 0 to H, we can get

$$\int_0^H \sum_{k=1}^{\infty} Y_k(0)\sin(\omega_k z)\ \sin(\omega_i z)\mathrm{d}z = \int_0^H u_0\sin(\omega_i z)\mathrm{d}z \tag{20}$$

According to the orthogonality of trigonometric function, we can obtain

$$Y_k(0) = \frac{2}{H}\int_0^H u_0\sin(\omega_k z)\mathrm{d}z \tag{21}$$

According to the model test, the time-temperature and loading functions are assumed as follows, respectively:

$$T(t) = a_0 + a_1\cdot\cos(w\cdot t) + b_1\cdot\sin(w\cdot t) \tag{22}$$

$$q(t)=\begin{cases} q_1 & 0\le t<t_1 \\ q_1+q_2 & t_1\le t<t_2 \\ q_1+q_2+q_3 & t\ge t_2 \end{cases} \tag{23}$$

where a_0, a_1, b_1, w are the constants in the model test temperature fitting function, and q_1 is the first level load applied at time 0, q_2 is the second level load applied at time t_1, q_3 is the third level load applied at time t_2.

Then $f(t)$ can be expressed as:

$$\begin{aligned} &f(t)=A_2\frac{\partial T(x,t)}{\partial t}+A_3\frac{\partial q(t)}{\partial t} \\ &=A_2\cdot w\cdot[-a_1\cdot\sin(w\cdot t)+b_1\cdot\cos(w\cdot t)]+A_3[q_1\cdot\delta(t)+q_2\cdot\delta(t-t_1)+q_3\cdot\delta(t-t_2)] \end{aligned} \tag{24}$$

where $\delta(t)$ is the Dirac function.

Then

$$\begin{aligned} \int_0^t e^{\frac{\omega_k^2}{A_1}\xi}\cdot f(\xi)\mathrm{d}\xi &= \int_0^t e^{\frac{\omega_k^2}{A_1}\xi}\cdot(A_2\cdot w\cdot[-a_1\cdot\sin(w\cdot\xi)+b_1\cdot\cos(w\cdot\xi)])\mathrm{d}\xi \\ &+\int_0^t e^{\frac{\omega_k^2}{A_1}\xi}\cdot(A_3[q_1\cdot\delta(\xi)+q_2\cdot\delta(\xi-\xi_1)+q_3\cdot\delta(\xi-\xi_2)])\mathrm{d}\xi \\ &=A_2\cdot w\cdot\left[-a_1\cdot\int_0^t e^{\frac{\omega_k^2}{A_1}\xi}\cdot\sin(w\cdot\xi)\mathrm{d}\xi+b_1\cdot\int_0^t e^{\frac{\omega_k^2}{A_1}\xi}\cdot\cos(w\cdot\xi)\mathrm{d}\xi\right] \\ &+A_3\cdot\int_0^t e^{\frac{\omega_k^2}{A_1}\xi}[q_1\cdot\delta(\xi)+q_2\cdot\delta(\xi-\xi_1)+q_3\cdot\delta(\xi-\xi_2)]\mathrm{d}\xi \\ =&\begin{cases} A_2\cdot w\cdot(-a_1\cdot jf_{s1}+b_1\cdot f_{c1})+A_3\cdot q_1 & 0\le t<t_1 \\ A_2\cdot w\cdot(-a_1\cdot f_{s1}+b_1\cdot f_{c1})+A_3\cdot\left(q_1+e^{\frac{\omega_k^2}{A_1}t_1}\cdot q_2\right) & t_1\le t<t_2 \\ A_2\cdot w\cdot(-a_1\cdot f_{s1}+b_1\cdot jf_{c1})+A_3\cdot\left(q_1+e^{\frac{\omega_k^2}{A_1}t_1}\cdot q_2+e^{\frac{\omega_k^2}{A_1}t_2}\cdot q_3\right) & t\ge t_2 \end{cases} \end{aligned} \tag{25}$$

where

$$\begin{cases} jf_{s1}=\int_0^t e^{\frac{\omega_k^2}{A_1}\xi}\cdot\sin(w\cdot\xi)\mathrm{d}\xi=\dfrac{A_1\left(w\cdot A_1+e^{\frac{\omega_k^2}{A_1}t}\left[-w\cdot A_1\cdot\cos(w\cdot t)+\omega_k^2\cdot\sin(w\cdot t)\right]\right)}{\omega_k^4+w^2\cdot A_1^2} \\ jf_{c1}=\int_0^t e^{\frac{\omega_k^2}{A_1}\xi}\cdot\cos(w\cdot\xi)\mathrm{d}\xi=\dfrac{-A_1\cdot\omega_k^2+A_1\cdot e^{\frac{\omega_k^2}{A_1}t}\left[\omega_k^2\cdot\cos(w\cdot t)+A_1\cdot w\cdot\sin(w\cdot t)\right]}{\omega_k^4+w^2\cdot A_1^2} \end{cases} \tag{26}$$

$$\begin{aligned} &Y_k(t)=-\frac{2}{H\cdot A_1\cdot\omega_k}\cdot e^{-\frac{\omega_k^2}{A_1}t}\int_0^t e^{\frac{\omega_k^2}{A_1}\xi}\cdot f(\xi)d\xi \\ &=-\frac{2}{H\cdot A_1\cdot\omega_k}\cdot\begin{cases} A_2\cdot w\cdot(-a_1\cdot JF_1+b_1\cdot JF_2)+e^{\frac{\omega_k^2}{A_1}(-t)}\cdot A_3\cdot q_1 & 0\le t<t_1 \\ A_2\cdot w\cdot(-a_1\cdot JF_1+b_1\cdot JF_2)+A_3\cdot\left(e^{\frac{\omega_k^2}{A_1}(-t)}\cdot q_1+e^{\frac{\omega_k^2}{A_1}(t_1-t)}q_2\right) & t_1\le t<t_2 \\ A_2\cdot w\cdot(-a_1\cdot JF_{s1}+b_1\cdot JF_2)+A_3\cdot\left(e^{\frac{\omega_k^2}{A_1}(-t)}\cdot q_1+e^{\frac{\omega_k^2}{A_1}(t_1-t)}q_2+e^{\frac{\omega_k^2}{A_1}(t_2-t)}q_3\right) & t\ge t_2 \end{cases} \end{aligned} \tag{27}$$

where

$$\begin{cases} JF_{s1}=e^{-\frac{\omega_k^2}{A_1}t}\cdot\int_0^t e^{\frac{\omega_k^2}{A_1}\xi}\cdot\sin(w\cdot\xi)\mathrm{d}\xi=\dfrac{A_1\left(w\cdot e^{-\frac{\omega_k^2}{A_1}t}\cdot A_1+\left[-w\cdot A_1\cdot\cos(w\cdot t)+\omega_k^2\cdot\sin(w\cdot t)\right]\right)}{\omega_k^4+w^2\cdot A_1^2} \\ JF_{c1}=e^{-\frac{\omega_k^2}{A_1}t}\cdot\int_0^t e^{\frac{\omega_k^2}{A_1}\xi}\cdot\cos(w\cdot\xi)\mathrm{d}\xi=\dfrac{-A_1\cdot e^{-\frac{\omega_k^2}{A_1}t}\cdot\omega_k^2+A_1\cdot\left[\omega_k^2\cdot\cos(w\cdot t)+A_1\cdot w\cdot\sin(w\cdot t)\right]}{\omega_k^4+w^2\cdot A_1^2} \end{cases} \tag{28}$$

The excess pore water pressure solution of a nonhomogeneous equation is briefly described as:

$$u(z,t) = \sum_{k=1}^{\infty} Y_k(t) \sin\left(\frac{2k-1}{2H}\pi x\right) = \sum_{k=1}^{\infty} Y_k(t) \sin(\omega_k z) \tag{29}$$

According to the principle of effective stress, the settlement caused by excess pore water pressure dissipation can be calculated as:

$$\begin{aligned} S_1(t) &= \int_0^H \frac{\sigma'}{E_s} \mathrm{d}z = \int_0^H \frac{\sigma_t - u}{E_s} \mathrm{d}z = \frac{q(t) \cdot H}{E_s} - \frac{1}{E_s} \int_0^H u(z,t) \mathrm{d}z \\ &= \frac{q(t) \cdot H}{E_s} - \frac{1}{E_s} \int_0^H \sum_{k=1}^{\infty} Y_k(t) \sin(\omega_k z) \mathrm{d}z \\ &= \frac{q(t) \cdot H}{E_s} - \frac{1}{E_s} \sum_{k=1}^{\infty} \frac{Y_k(t)}{\omega_k} \end{aligned} \tag{30}$$

The vertical deformation caused by variation in temperature can be calculated as:

$$S_2(t) = \alpha_s \cdot T(t) \cdot H \tag{31}$$

The total settlement of the soil layer can be obtained as follows:

$$S(t) = S_1(t) - S_2(t) \tag{32}$$

4.4. Calculation and Verification

The calculation was carried out for verification by comparing with the testing findings, in accordance with the proposed solutions. The deterministic clay parameters in the case are listed in Table 2.

Table 2. The deterministic parameters of clay.

Parameter	Value	Parameter	Value
k_w (m/s)	2×10^{-9}	α_s (/°C)	1.5×10^{-5}
γ_w (kN·m^{-3})	9.8	α_w (/°C)	2.0×10^{-4}
E_s (MPa)	0.9	K_s (GPa)	20.1
n	0.55	K_w (GPa)	5.07
H (m)	1	K_0 (MPa)	7.02

The multi-stage loading was taken as q_1 = 2.5 kPa, q_2 = 10 kPa, q_3 = 12.5 kPa based on the testing. Assuming that the temperature distribution was uniform throughout the entire clay layer, the temperature fluctuations over time were taken into account. The T(t) temperature change function was obtained by fitting the average temperature change curve of the total layer as shown in Figure 12. The function was expressed as follows:

$$\begin{aligned} T(t) = a_0 + a_1 \cdot \cos(t \cdot w) + b_1 \cdot \sin(t \cdot w) + a_2 \cdot \cos(2t \cdot w) + b_2 \cdot \sin(2t \cdot w) + \\ a_3 \cdot \cos(3t \cdot w) + b_3 \cdot \sin(3t \cdot w) + a_4 \cdot \cos(4t \cdot w) + b_4 \cdot \sin(4t \cdot w) \end{aligned} \tag{33}$$

where $a_0 = -254$, $a_1 = -203.2$, $b_1 = 550.5$, $a_2 = 476.1$, $b_2 = 176.6$, $a_3 = 48.95$, $b_3 = -255.9$, $a_4 = -61.18$, $b_4 = 5.957$, $w = 0.06228$.

Figures 13 and 14, respectively, compare excess pore water pressure and settlements between testing and calculating results. The fitted curve depicts the significant temperature change trend when compared to the actual temperature change. Therefore, the theoretical calculated values of excess pore water pressure dissipation have no significant fluctuations. The measured settlement hardly increased at the end of each stage, but the theoretical calculating curve continues to show a trend of continuous growth. This is mostly caused by the model tank wall's friction resistance during loading. Furthermore, it is evident from analytical calculations that solar heating indeed results in greater settlement.

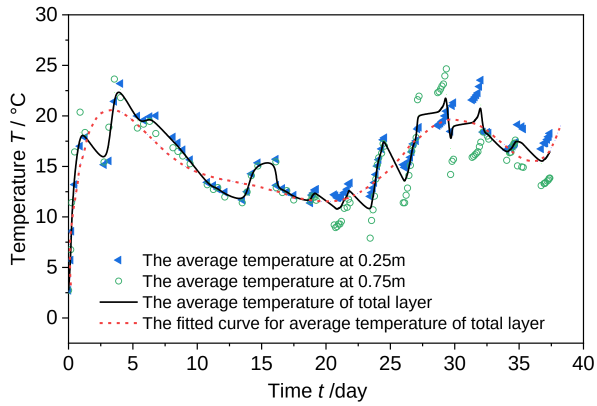

Figure 12. The temperature fitted curve.

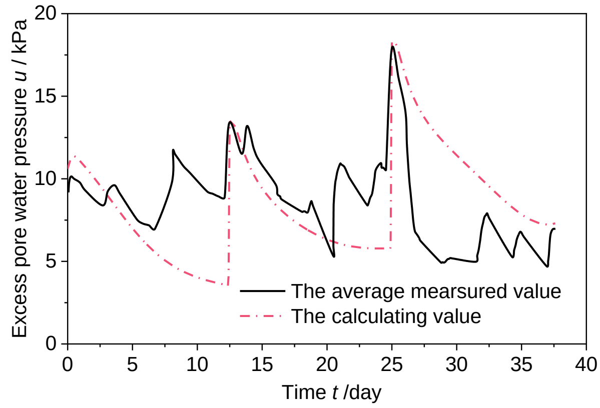

Figure 13. Comparison of excess pore water pressure in solar heating group.

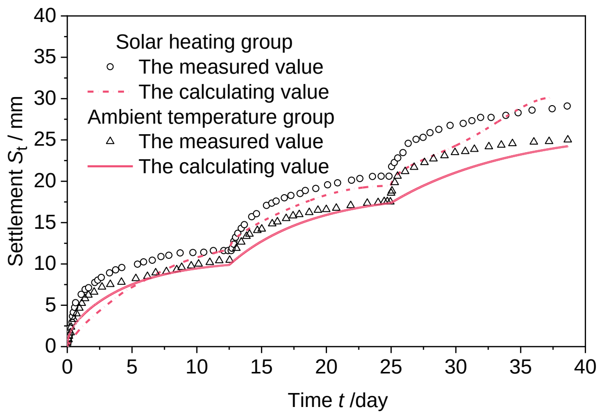

Figure 14. Comparison of settlements between testing and calculating values.

5. Conclusions

In this paper, a model test for one-dimensional thermal consolidation using solar energy was conducted to investigate the effect of the novel foundation treatment technology, and an analytical calculation method was proposed for predicting the consolidation behavior. The conclusions are as follows:

1. The range of temperature variation is minimal and the average soil temperature in the ambient temperature group is not far from the daily mean ambient temperature. Solar heating can raise the foundation temperature by 15 °C when it is used in winter and greatly widen the day's temperature variation range. The variance in soil temperature over the course of a single day can exceed 10 °C.

2. The development of excess pore water pressure is related to the sun. It begins to increase as the sun rises and reaches its peak as the sun is ready to set. The average daily excess pore water pressure increased by solar heating is 2.5 kPa, and the maximum increment is 6.8 kPa. Solar heating can improve the consolidation effect in the deep foundation, because it causes the thermal expansion of the pore water and clay skeleton, leading to an increase in the total stress under the constraint of lateral displacement.
3. The solar heating group's settlement was 16% higher than the ambient group's. With the progress of consolidation, the impact of solar heating on the accelerating settlement steadily increased. On account of the consolidation and thermal contraction of the clay during the night, the settlement rate increased all night, but dropped during the day.

Author Contributions: Conceptualization, C.X., Y.D., M.Z. and X.C.; methodology, C.X., Y.D. and M.Z.; software, C.X. and Y.D.; validation, M.Z. and J.N.; formal analysis, M.Z.; investigation, C.X., Y.D. and M.Z.; resources, C.X. and Y.D.; data curation, L.Z.; writing—original draft preparation, C.X.; writing—review and editing, M.Z., J.N. and L.Z.; visualization, M.Z. and J.N.; supervision, C.X., Y.D. and M.Z.; project administration, C.X., M.Z. and X.C.; funding acquisition, C.X., M.Z. and X.C. All authors have read and agreed to the published version of the manuscript.

Funding: This research was funded by the China Postdoctoral Science Foundation, grant number 2021T140475; the National Natural Science Foundation of China, grant number 52108329, grant number 52008263, grant number 52090084, and grant number 51908371; the Shenzhen Science and Technology Program, grant number KQTD20200909113951005.

Institutional Review Board Statement: Not applicable.

Informed Consent Statement: Not applicable.

Data Availability Statement: Data is contained in the article.

Conflicts of Interest: The authors declare no conflict of interest.

References

1. Abuel-Naga, H.M.; Bergado, D.T.; Chaiprakaikeow, S. Innovative thermal technique for enhancing the performance of prefabricated vertical drain during the preloading process. *Geotext. Geomembr.* **2006**, *24*, 359–370. [CrossRef]
2. Artidteang, S.; Bergado, D.T.; Saowapakpiboon, J.; Teerachaikulpanich, N.; Kumar, A. Enhancement of efficiency of prefabricated vertical drains using surcharge, vacuum and heat preloading. *Geosynth. Int.* **2011**, *18*, 35–47. [CrossRef]
3. Deng, Y.B.; Liu, G.B.; Indraratna, B.; Rujikiatkamjorn, C.; Xie, K.H. Model test and theoretical analysis for soft soil foundations improved by prefabricated vertical drains. *Int. J. Geomech.* **2017**, *17*, 04016045. [CrossRef]
4. Finn, F. The effect of temperature on the consolidation characteristics of remolded clay. In *Symposium on Consolidation Testing of Soils*; ASTM International: West Conshohocken, PA, USA, 1952.
5. Hillel, D. *Fundamentals of Soil Physics*; Academic Press: New York, NY, USA, 1980.
6. Abuel-Naga, H.M.; Bergado, D.T.; Ramana, G.V.; Grino, L.; Rujivipat, P.; Thet, Y. Experimental evaluation of engineering behavior of soft Bangkok clay under elevated temperature. *J. Geotech. Geoenviron. Eng.* **2006**, *132*, 902–910. [CrossRef]
7. Tsutsumi, A.; Tanaka, H. Combined effects of strain rate and temperature on consolidation behavior of clayey soils. *Soils Found.* **2012**, *52*, 207–215. [CrossRef]
8. Jaradat, K.A.; Abdelaziz, S.L. Thermo-mechanical behavior of saturated clays using discrete element modelling. In *Geo-Congress 2019: Geotechnical Materials, Modeling, and Testing*; American Society of Civil Engineers: Reston, VA, USA, 2019; pp. 125–134.
9. Campanella, R.G.; Mitchell, J.K. Influence of temperature variations on soil behavior. *J. Soil Mech. Found. Div.* **1968**, *94*, 709–734. [CrossRef]
10. Houston, S.L.; Houston, W.N.; Williams, N.D. Thermo-mechanical behavior of seafloor sediments. *J. Geotech. Eng.* **1985**, *111*, 1249–1263. [CrossRef]
11. Abuel-Naga, H.M.; Bergado, D.T.; Bouazza, A. Thermally induced volume change and excess pore water pressure of soft Bangkok clay. *Eng. Geol.* **2007**, *89*, 144–154. [CrossRef]
12. Towhata, I.; Kuntiwattanaku, P.; Seko, I.; Ohishi, K. Volume change of clays induced by heating as observed in consolidation tests. *Soils Found.* **1993**, *33*, 170–183. [CrossRef]
13. Delage, P.; Sultan, N.; Cui, Y.J. On the thermal consolidation of Boom clay. *Can. Geotech. J.* **2000**, *37*, 343–354. [CrossRef]
14. Bai, B. Thermal consolidation of layered porous half-space to variable thermal loading. *Appl. Math. Mech.-Engl. Ed.* **2006**, *27*, 1531–1539. [CrossRef]
15. Ai, Z.Y.; Wang, L.J. Axisymmetric thermal consolidation of multilayered porous thermoelastic media due to a heat source. *Int. J. Numer. Anal. Methods Geomech.* **2015**, *39*, 1912–1931. [CrossRef]

16. Tao, H.B.; Liu, G.B.; Xie, K.H. A constitutive model for thermal consolidation with vertical drains and its experimental verification. *Chin. J. Geotech. Eng.* **2015**, *37*, 1077–1085.
17. Deng, Y.B.; Wang, T.Y.; Kong, G.Q. Consolidation theory for saturated ground considering temperature effects. *Chin. J. Geotech. Eng.* **2019**, *41*, 1827–1835.
18. Morteza Zeinali, S.; Abdelaziz, S.L. Thermal consolidation theory. *J. Geotech. Geoenviron. Eng.* **2021**, *147*, 04020147. [CrossRef]
19. Wang, L.; Wang, L. Semianalytical analysis of creep and thermal consolidation behaviors in layered saturated clays. *Int. J. Geomech.* **2020**, *20*, 06020001. [CrossRef]
20. Pothiraksanon, C.; Bergado, D.T.; Abuel-Naga, H.M. Full-scale embankment consolidation test using prefabricated vertical thermal drains. *Soils Found.* **2010**, *50*, 599–608. [CrossRef]
21. Bai, B.; Zhang, P.; Jia, D. The consolidation effects of a saturated red clay subjected to temperature loading with different amplitudes. *Chin. J. Geotech. Eng.* **2013**, *35*, 1972–1978.
22. Bai, M.; Abousleiman, Y. Thermoporoelastic coupling with application to consolidation. *Int. J. Numer. Anal. Methods Geomech.* **1997**, *21*, 121–132. [CrossRef]
23. Liu, Q.; Deng, Y.B.; Wang, T.Y. One-dimensional nonlinear consolidation theory for soft ground considering secondary consolidation and the thermal effect. *Comput. Geotech.* **2018**, *104*, 22–28. [CrossRef]
24. Niu, J.; Wang, X.; Gong, S.; Ling, D. Exact solutions for investigating thermal response of saturated soil induced by temperature change. *Int. J. Geomech.* **2020**, *20*, 04020177. [CrossRef]
25. Tao, H.; Xie, K.; Liu, G.; Huang, D.; Deng, Y. Finite Element Analysis of Foundation Consolidation by Vertical Drains Coupling Thermo-Hydro-Mechanical Effect. *Rock Soil Mech.* **2013**, *34*, 494–500. [CrossRef]
26. Hueckel, T.; Baldi, G. Thermoplasticity of saturated clays: Experimental constitutive study. *J. Geotech. Eng.* **1990**, *116*, 1778–1796. [CrossRef]
27. Hueckel, T.; Borsetto, M. Thermoplasticity of saturated soils and shales: Constitutive equations. *J. Geotech. Eng.* **1990**, *116*, 1765–1777. [CrossRef]
28. Hueckel, T.; Pellegrini, R.; Del Olmo, C. A constitutive study of thermo-elasto-plasticity of deep carbonatic clays. *Int. J. Numer. Anal. Methods Geomech.* **1998**, *22*, 549–574. [CrossRef]
29. Cekerevac, C.; Laloui, L. Experimental study of thermal effects on the mechanical behaviour of a clay. *Int. J. Numer. Anal. Methods Geomech.* **2004**, *28*, 209–228. [CrossRef]
30. Abuel-Naga, H.M.; Bergado, D.T.; Bouazza, A.; Ramana, G.V. Volume change behaviour of saturated clays under drained heating conditions: Experimental results and constitutive modeling. *Can. Geotech. J.* **2007**, *44*, 942–956. [CrossRef]
31. Ai, Z.Y.; Wang, L.J. Precise solution to 3D coupled thermohydromechanical problems of layered transversely isotropic saturated porous media. *Int. J. Geomech.* **2018**, *18*, 04017121. [CrossRef]
32. Coccia, C.J.R.; McCartney, J.S. Thermal volume change of poorly draining soils II: Model development and experimental validation. *Comput. Geotech.* **2016**, *80*, 16–25. [CrossRef]
33. Wen, M.; Tian, Y.; Li, L.; Qiu, X.; Wang, K.; Wu, W.; Mei, G.; Xu, M. A general interfacial thermal contact model for consolidation of bilayered saturated soils considering thermo-osmosis effect. *Int. J. Numer. Anal. Methods Geomech.* **2022**, *46*, 2375–2397. [CrossRef]
34. Yang, G.; Liu, Y.; Chen, P. Thermal Consolidation of Saturated Silty Clay Considering Different Temperature Paths: Experimental Study and Constitutive Modeling. *Int. J. Geomech.* **2022**, *22*, 04021293. [CrossRef]
35. Sun, D.A.; Xue, Y.; Wang, L. Analysis of one-dimensional thermal consolidation of saturated soil considering heat conduction of semi-permeable drainage boundary under varying loading. *Rock Soil Mech.* **2020**, *41*, 1465–1473. [CrossRef]